J. Water Environ. Nanotechnol., 8(2): 137-150 Spring 2023

ORIGINAL RESEARCH PAPER

Characterizations of synthesized laser-scribed graphene/ molybdenum disulfide (LSG/MoS_2) hybrids for supercapacitor performance

Mugashini Vasudevan[1,2], Aiswarya Kanesan[2], Sathaniswarman Remesh[1,2], Veeradasan Perumal[1,2], Pandian Bothi Raja[3], Mohamad Nasir Mohamad Ibrahim [3], Saravanan Karuppanan[2], Subash C.B. Gopinath[4,5] and Mark Ovinis[6]

[1]Centre of Innovative Nanostructures and Nanodevices (COINN), Universiti Teknologi PETRONAS, 32610 Seri Iskandar, Perak Darul Ridzuan, Malaysia
[2]Department of Mechanical Engineering, Universiti Teknologi PETRONAS, 32610 Seri Iskandar, Perak Darul Ridzuan, Malaysia
[3]School of Chemical Sciences, Universiti Sains Malaysia, 11800, Penang, Malaysia
[4]Institute of Nano Electronic Engineering, Kangar 01000 & Faculty of Chemical Engineering & Technology, Arau 02600, Universiti Malaysia Perlis (UniMAP), Perlis, Malaysia
[5]Micro System Technology, Centre of Excellence (CoE), Universiti Malaysia Perlis (UniMAP), 02600 Arau, Pauh Campus, Perlis, Malaysia.
[6]School of Engineering and the Built Environment, Faculty of Computing, Engineering, and the Built Environment, Birmingham City University, B4 7XG, UK

Received: 2023-01-14 Accepted: 2023-03-28 Published: 2023-05-17

ABSTRACT
A sustainable and organic energy storage system from oil palm lignin waste-derived laser-scribed graphene embedded with molybdenum disulfide (LSG/MoS_2) is reported in this work. LSG/MoS_2 hybrids were fabricated to overcome the zero-band gap of graphene, and molybdenum disulfide restacking issues, and to induce electrical conductivity. Various amounts of LSG (0.1,0.5,1.0 g) were added in a MoS_2 precursor to produce a nanoscale LSG/MoS_2 hybrid nanostructure via the hydrothermal method. The Raman D, G, and 2D bands of LSG confirmed the formation of graphene from lignin. The FESEM morphology of LSG/MoS_2 hybrids showed a porous and large surface area anchored with 3D MoS_2 nanoflower on LSG. TEM imaging revealed MoS_2 decorated LSG with a lattice spacing of 0.62 and 0.27nm, corresponding to the (002) and (100) planes of MoS_2. In terms of electrochemical performance, LSG with 0.1g of MoS_2 has the lowest resistance, the highest specific capacitance of 6.7mF/cm^2 at 0.05 mA/cm^{2,} and excellent cyclic stability of 98.1% over 1000 cycles, based on Electrochemical Impedance Spectroscopy (EIS), Cyclic Voltammetry (CV) and Galvanostatic Charge Discharge (GCD) tests.

Keywords: Oil palm lignin; molybdenum disulfide; morphological; structural; supercapacitor

How to cite this article
Vasudevan M., Kanesan A., Remesh S., Perumal V., Bothi Raja P., Mohammad Ibrahim M. N., Karuppanan S., Gopinath S. C. B., Ovinis M., Characterizations of synthesized laser-scribed graphene/molybdenum disulfide (LSG/MoS2) hybrids for supercapacitor performance. J. Water Environ. Nanotechnol., 2023; 8(2): 137-150 DOI: 10.22090/jwent.2023.02.004

INTRODUCTION

Green energy is an efficient and effective alternative to energy generated from the combustion of fossil fuels. It is clean, sustainable, safe, and renewable, and many countries have committed to reducing their carbon footprint by 2030 [1] by using green energy as an alternative energy source. Some examples of green energies used around the world are wind, hydrothermal, solar, and geothermal energy.

Energy storage is crucial to balance the supply

* Corresponding Authors Email: *veeradasan.perumal@utp.edu.my*

and demand of energy. To decrease the imbalances between the demand for energy and the production of energy, energy storage systems (ESSs) are used to capture energy produced for use later. Most commonly, electrochemical power sources such as batteries are used for energy storage. Alternatively, supercapacitors, which have lower cost, longer cycle life, higher power density, rapid charge/discharge, and are environmentally friendly, may be used [2]. There are three categories of supercapacitors: Electrochemical Double-Layer Capacitors (EDLC), which are a carbon material that is formed due to the separation of charge at the electrode/electrolyte interface, pseudocapacitors that uses fast charge transfer through a redox process using transition metal oxides to store energy and conducting polymers and hybrid capacitors which combine both the EDLC and pseudocapacitors [3].

Carbon-based material like graphene has been widely used in supercapacitor applications, as graphene has a large specific surface area, making it an ideal supercapacitor electrode material [4]. Conventionally, graphene is synthesized using coal, a non-renewable source, through mechanical exfoliation, chemical exfoliation, and chemical vapor deposition (CVD). However, these techniques have several drawbacks, such as precise synthesis condition requirements, high temperatures, high cost, high energy, environmentally harmful to the environment, and time-consuming.

Laser scribing solves all these drawbacks as it is simple, cost-effective, and requires less precise synthesis conditions [5]. Z. Wan et al. reviewed laser-scribed graphene for supercapacitors [6] and found that laser-scribed graphene has unique properties such as flexible fabrication, large surface area, and high electrical conductivity. A flexible graphene-based supercapacitor electrode can be synthesized from polyimide sheets through laser scribing. However, the fabrication of graphene from polyimide is not environmentally friendly, requiring large resources and polyimide waste after the service lifetime. In that regard, lignin biopolymer is a viable alternative to polyimide and coal in synthesizing graphene [7]. Lignin is a biopolymer that is abundant in plants. It has high carbon content and aromatic subunits. Apart from cellulose and hemicellulose, lignin is naturally found in biomass. Nevertheless, lignin has an amorphous nature that limits electrical conductivity. 135 million tons of oil palm waste is generated in Malaysia annually [8,9]. Lignin extracted from oil palm waste was scribed through a carbon dioxide laser scribing process to fabricate eco-friendly graphene as reported by Naidu Loganathan N et al [7]. The graphene-derived oil palm lignin has limited electrical properties as it is not up to the standard of commercial graphene.

MoS_2 has a unique sandwich structure of triple hexagonal layers of S-Mo-S and is used for the fabrication of electrodes due to its low cost, non-toxicity, abundance, high specific capacitance, high chemical stability, excellent electrocatalytic properties, and good cyclic performance [10–12]. It is a promising transition metal dichalcogenide with wide-ranging potential applications in energy storage devices nanoelectronics, biosensors, and supercapacitors. Various transition metal dichalcogenides nanostructures, such as manganese diselenide, titanium disulfide, and tungsten disulfide nanostructure, have been incorporated in the electrodes of EDLC and hybrid capacitors. A manganese-doped MoS_2 supercapacitor was reported by I.T.Bello et al. with a specific capacitance of 70.37 Fg^{-1}[13]. M.A. Bissett et al. reported that the conjugation of graphene with MoS_2 improves specific capacitance through morphology alteration and resistivity reduction [14]. S.K. Asl et al. synthesized a MoS2-decorated graphene supercapacitor with a specific capacitance of ~ 8 Fcm^{-3} through a laser scribing method. Graphene oxide and MoS_2 were chemically mixed, coated on a light-scribed DVD, and lasered [15]. M.M. Baig et al. obtained a specific capacitance of 850 F/g with MoS_2 nanoflowers on reduced graphene oxide, forming a nanohybrid through a hydrothermal process, [16]. Another study reported that nickel oxide nanoparticles incorporated with MoS_2 and reduced graphene oxide enhance charge transfer behavior and the corresponding capacitance. The MoS_2/reduced graphene oxide/nickel oxide nanoparticles composite has a capacitance of 7.38 $mFcm^{-2}$ [17].

In this study, we have synthesized graphene from oil palm lignin similar to the reported article by Naidu Loganathan N et al [7]. Thus, we have grown MoS_2 on modified laser-scribed graphene through a hydrothermal process. The formation of LSG/MoS_2 hybrid overcomes the drawback of lignin-based graphene in terms of limitation in electrical properties and also the severe stacking issue of MoS_2. The severe stacking and restacking problems of MoS_2 were due to the unstable van der Waals interaction, which significantly reduces

its active sites and causes poor energy density. In that regard, hybrid material bonding with MoS_2 is necessary. The coupling of LSG/MoS_2 forming a hybrid performs higher specific capacitance than the reported specific capacitance by Naidu Loganathan N et al. It should be taken note that the current experiment setup is conducted at a different voltage range due to the presence of a composite material. A new result has been given by the current electrode as it can run as both positive and negative electrodes at different voltage ranges. Moreover, the addition of MoS_2 to LSG has increased the capacitance to 3-fold due to higher electrical conductivity and higher surface area of produced MoS_2 nanoflower. Carbon-based materials comprising hybrid capacitors and transition metal dichalcogenides were used as electrode material due to their large specific capacitance, and weak van der Waals force, for improved greater energy density and specific capacitance.

MATERIALS AND METHODOLOGY

Materials

Lignin extracted from an oil palm empty fruit bunch was purified [18] for conversion to graphene. Chemicals such as carbon black, sulphuric acid (H_2SO_4), polyvinylidene fluoride (PVDF), N-methyl-2-pyrrolidinone (NMP), sodium molybdate dehydrate, thiourea, and ethanol absolute were obtained from Merck & Co. All these chemicals were used as received, without additional purification. Screen-Printed Carbon Electrodes (SPCE) were purchased from Metrohm (Malaysia) Sdn. Bhd.

Synthesis of lignin-based graphene through laser scribing technique

Firstly, a 20% concentration lignin solution was prepared by adding 20 grams of lignin powder into 100 milliliters of distilled water. The solution was stirred using a magnetic stirrer for 30 minutes on a hot plate until a homogenous lignin solution was formed. Then, the lignin solution was coated on a laboratory glass substrate through the drop coat method and let to dry in an oven at 50°C for 20 minutes. The dried lignin on the glass substrate was allowed to cool for 2 minutes before adding the second layer to the same glass substrate. This step was repeated until five layers of lignin were coated on the glass substrate successfully. Next, the dried lignin-coated glass substrate was placed in a laser scribe machine. The laser scribe parameters were set to 50% laser speed, 50% laser power, and 500% pulse per inch. CO_2 laser penetrated the lignin-coated glass substrate forming graphene after 30 minutes with the brown lignin turned into black graphene. The graphene was collected and placed in a desiccator to avoid contamination.

Preparation of modified laser-scribed graphene (LSG)

The lignin-based graphene is insoluble in water due to carbon atoms. Therefore, to increase the solubility of the laser-scribed graphene, carbon black was added to improve the electrode conductivity and accessibility of electrolyte-electrode, polyvinylidene fluoride (PVDF). This is to enhance the thermal stability with N-methyl-2-pyrrolidinone (NMP) acting as a homogenizer and aiding dissolution. PVDF is the only polymer that can be used to fabricate an electrochemical device that acts as a binder, separator, electrolyte, and piezoelectricity generator [19]. The polymeric binder properties of PVDF improve the mechanical strength of lignin-based graphene, which directly influences the supercapacitor performance [20]. Carbon black conversely, acts as a conductive additive to improve the electrical properties of lignin-based graphene [21]. Lignin-derived graphene, carbon black, and PVDF were mixed in a ratio of 75:15:10, equivalent to 150 milligrams of lignin-derived graphene, 30 milligrams of carbon black, and 20 milligrams of PVDF. The ratio for LSG preparation was taken from a previously reported work [22] with a slight modification. Next, NMP was added to the mixture to form a semi-fluidic slurry product through sonication.

Fabrication of laser-scribed graphene/molybdenum disulfide (LSG/MoS_2)

LSG/MoS_2 was prepared by dissolving 0.1 grams of modified LSG, 0.6 grams of sodium molybdate dehydrate, and 1.77 grams of thiourea in 60 milliliters of distilled water [23,24]. The mixture was stirred using a magnetic stirrer for 1 hour at room temperature on a hot plate at 1000 rpm. After a homogenous solution of MoS_2 was obtained, the MoS_2 was transferred into 250-millilitre Teflon-lined stainless-steel autoclave. Then, for smooth fabrication, 60% of the total volume of the Teflon-lined stainless-steel autoclave was filled with distilled water, equal to 90 milliliters. The Teflon chamber was closed to form an air-tight seal before placing it in the oven for a hydrothermal process

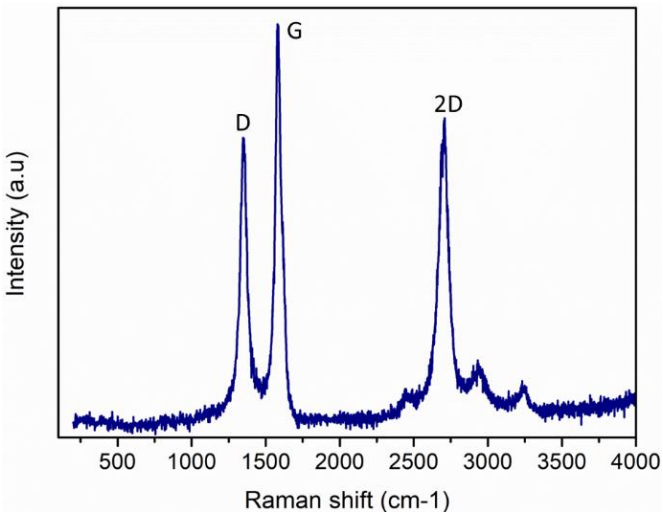

Fig. 1: Raman Spectroscopy of LSG at a speed of 50% and laser power of 50%.

at 200°C for 24 hours. After the hydrothermal process, the Teflon autoclave was cooled for 4 to 5 hours. Black precipitates of LSG/MoS_2 were produced during the hydrothermal process. The precipitates were washed thrice using absolute ethanol and distilled water simultaneously through centrifugation. After centrifugation, the product was dried in an oven at 60°C for 12 hours. The same procedure was repeated with 0.5 grams and 1.0 grams of modified LSG [25]. Also, pure MoS_2 was fabricated without adding complex LSG into the hydrothermal mixture. The LSG/MoS_2 hybrid was classified as LSG/ MoS_2-0.1, LSG/ MoS_2-0.5, and LSG/ MoS_2-1.0, according to the amount of LSG added.

Characterization

Field Emission Scanning (VP-FESEM) (Carl Zeiss SUPRA55 VP, Gemini) and Transmission Electron Microscopy (TEM) (HITACHI HT 7830) imaging, Raman spectroscopy (HORIBA Jobin Yvon HR800), X–ray diffraction (XRD) (X'Pert3 Powder & Empyrean, PANalytical with a Cu Kα radiation (λ=1.54 Å)), X-ray photoelectron spectroscopy (XPS) (Thermo Scientific K-Alpha), and Fourier Transform Infrared Spectroscopy (FT-IR) (Brand: Pelkin Elmer Inc, Spectrum One/ BX) were carried out to determine the morphological, chemical states and optical properties of the fabricated laser scribed materials. Electrochemistry Impedance Spectra (EIS), Cyclic Voltammetry (CV), and Galvanostatic charge and discharge (GCD) tests were carried out through Metrohm Multi Autolab M204 Potentiostat/Galvanostat. CV and GCD tests were performed using 1M H_2SO_4 solution.

RESULTS AND DISCUSSION

Raman Spectroscopy

Raman Spectroscopy of the fabricated laser-scribed graphene's structure, quality, and crystalline size. revealed 3 bands: D, G, and 2D. The bands were identified and evaluated based on acceptable ranges to validate the presence of laser-scribed graphene. Based on Fig. 1, the first peak with a value of 1327.52 cm^{-1} was identified as a D band due to the structural defects or partially disordered graphitic domains and lattice distortions of graphene basal planes [26]. During the laser scribing procedure, uneven laser power and speed may have caused the identified D peak.

Furthermore, the presence of lignin within the graphene sheet might be another defect, causing the D peak to develop. The D peak may be caused by the edge of the laser scribe graphene. The second peak at 1581.32 cm^{-1} is considered a G band, confirming the presence of graphitic carbon that corresponds to the first-order scattering of graphite's sp^2 mode [26,27]. When high-quality graphene is generated at optimal power and speed, the intensity of the G peak will rise. The last peak found was the 2D band, which confirms the restorations of sp^2 hybridized carbon-carbon bonds in graphitic structure and the development of stacked multiple graphenes after reduction [4]. The effective thickness of the graphene layer and quality of graphene can

be calculated using I_G / I_{2D} (0.5845) and I_D / I_G (0.8521). The crystalline structure's value can be calculated using the equation below:

$$La = 2.4 \times 10^{-10} \times laser\ wavelength^4 \times (ID / IG)^{-1}$$

The calculated crystalline structure La showed a value of 1.5497 E^{-7}. The use of a lignin concentration of 20% with 50% laser power and speed is more effective in recovering the sp_2 network graphite structure of the LSG than conventional methods [27,28]. To confirm these findings, FESEM was carried out to examine the surface morphology of LSG.

Field-Emission Scanning Electron Microscopy (FESEM)

Fig. 2 shows the surface morphology of the fabricated LSG/MoS_2 hybrids, LSG, and pure MoS_2. The LSG/MoS_2 hybrids were synthesized through hydrothermal technique with various amounts of LSG added, classified as LSG/MoS_2-0.1, LSG/MoS_2-0.5, and LSG/MoS_2-1.0, respectively. Fig. 2(a-f) shows uniform MoS_2 nanoflower anchoring around the surface of the fabricated LSG foam-like nanostructure in all three cases. As shown in Fig. 2(a & b), the shape and size of the MoS_2 nanoflower formed around the LSG/MoS_2-0.1 hybrid nanostructure were not uniform and aggregated. As for Fig. 2(c & e), the presence of LSG can be observed only in a few places, with the amount of LSG affecting the morphology structure. LSG is abundant in the LSG/MoS_2-1.0 hybrid nanostructure, as shown in Fig. 2(e & f). The LSG with mesopores has a large surface area which can boost electrochemical performance. The close-up view of the LSG/MoS_2 composite in Fig. 2(f) shows the incorporation of MoS_2 nanoflower onto the LSG nanofoam. The MoS_2 and LSG nanostructure are entwined to form an interconnected conductive network with a relatively smooth surface, which ensures optimum accessibility of electrolyte ions due to the hydrothermal process [29].

The heterogeneous growth of the MoS_2 nanoflower on LSG nanostructure results in a larger diameter, with dense MoS_2 nanoflower with significant active side edge exposure compared to the hybrid of nanoflowers of other concentrations. The 3D nanostructure also enhanced the stability of the LSG/ MoS_2-1.0 composite due to the strength of LSG, reducing the agglomeration [30]. The LSG/MoS_2 nanostructure was fabricated without any binder and conducting agent with abundant mesopores is beneficial to providing a 3D network for enhanced the electron transferred and can shorten the electron transport distance, leading to stable performance of the supercapacitor. Fig. 2(a-f) proves that as the amount of graphene increase, the surface area of the nanomaterial increase, resulting in enhanced electrochemical performance of the material respectively. Fig. 2(g & h) shows the morphology of LSG. At low FESEM magnification, the LSG material has a foam-like appearance, with overlying elongated nanograin-like structures. The foam-like appearance is caused by the release of gas during the laser scribing process, causing chemical bonds to break sublimed atoms and recombine into gaseous products, which find their way out of the structure through the generation of pores [31,32]. LSG becomes highly porous when converting lignin into LSG, mainly due to carburizing. The sp^3 carbon atom in the lignin molecule will be converted to the sp^2 carbon atom due to heat produced by the laser machine. The oxygen will be mainly removed from graphene oxide to form reduced graphene oxide with a 3D structure during carbonization.

As shown in Fig. 2h, the LSG has a large surface area with porous structures with different diameters. This structure induces the binding of nanoparticles that improves the diffusion of ions to the electrode from electrolyte and mass transportation during the electrochemical performance. The FESEM images of MoS_2 can be observed in Fig. 2(i & j). In Fig. 2(i), the MoS_2 formed in sheets due to its intrinsic lamellar structure. Weak Van der Waals interaction causes these sheets to clump, forming three-dimensional MoS_2 nanoflower, as shown in Fig. 2(j). Furthermore, the growth and size ranging below 200 nm of MoS_2 are similar. These fabricated materials have unique properties, which can induce physiochemical performance for supercapacitor applications.

Transmission Electron Microscopy (TEM)

The structural morphology of the MoS_2-decorated on LSG was further examined under TEM. Fig. 3(a & b) reveals that the MoS_2 nanoflower was homogeneously distributed on the graphene resulting in the strong interaction of MoS_2 on LSG [33]. Furthermore, the graphene sheets show a strong ability to prevent the aggregation of MoS_2 nanosheets, increasing the active area. Fig. 3(c) is a high-resolution TEM image taken along the edge part of these composites. Stripe-like grains with ~20 nm in length and several nanometres

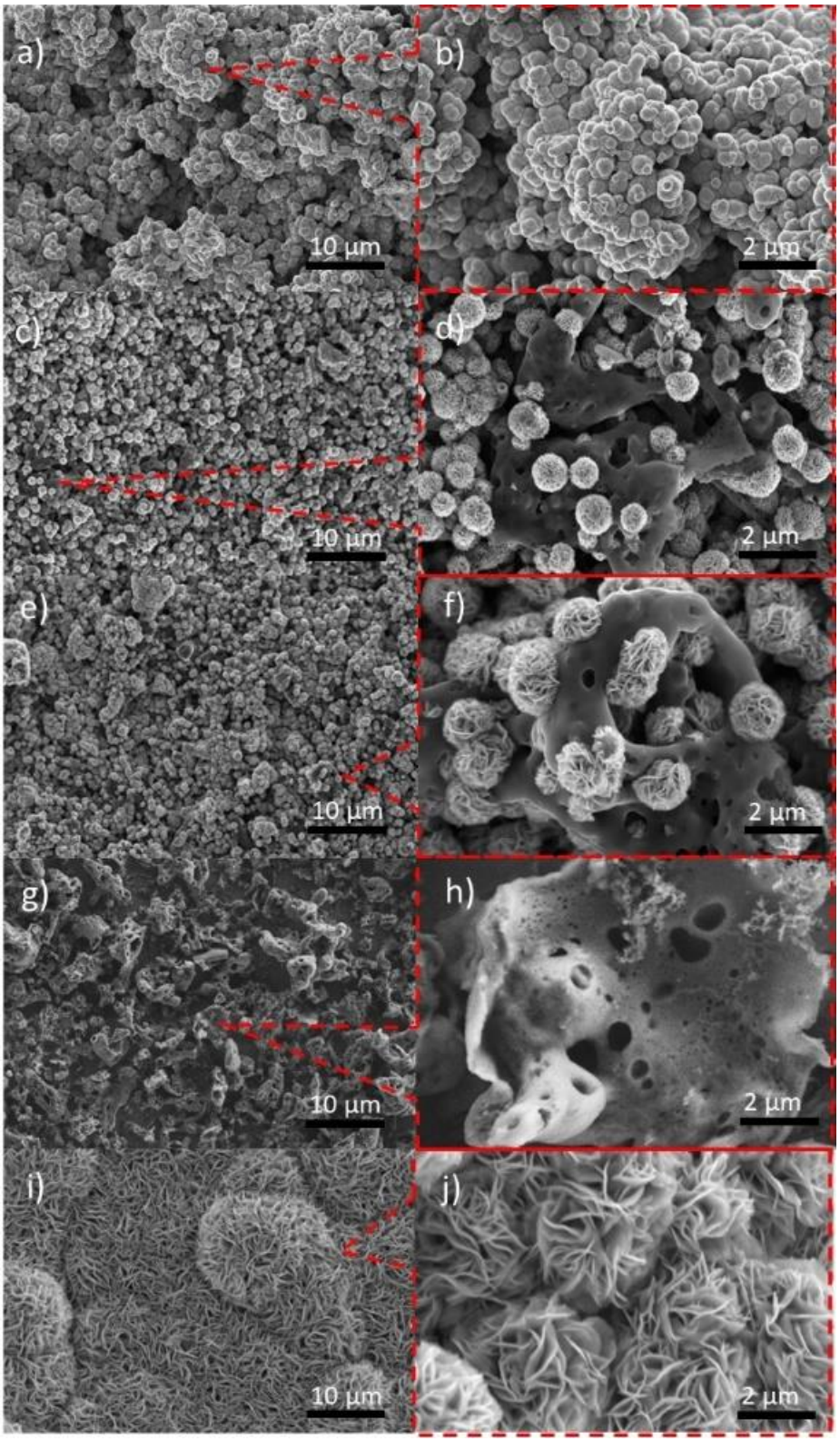

Fig. 2: FESEM images of f LSG/MoS_2 hybrids nanostructures (a) Low and (b) high magnifications images of LSG/MoS_2-0.1; (c) Low and (d) high magnifications of LSG/MoS_2-0.5 and (e) Low and (f) high magnifications of LSG/MoS_2-1.0. FESEM images of (g) Low and (h) high magnifications of LSG. FESEM images of (i) Low and (j) high magnifications of pure MoS_2 nanoflower were shown.

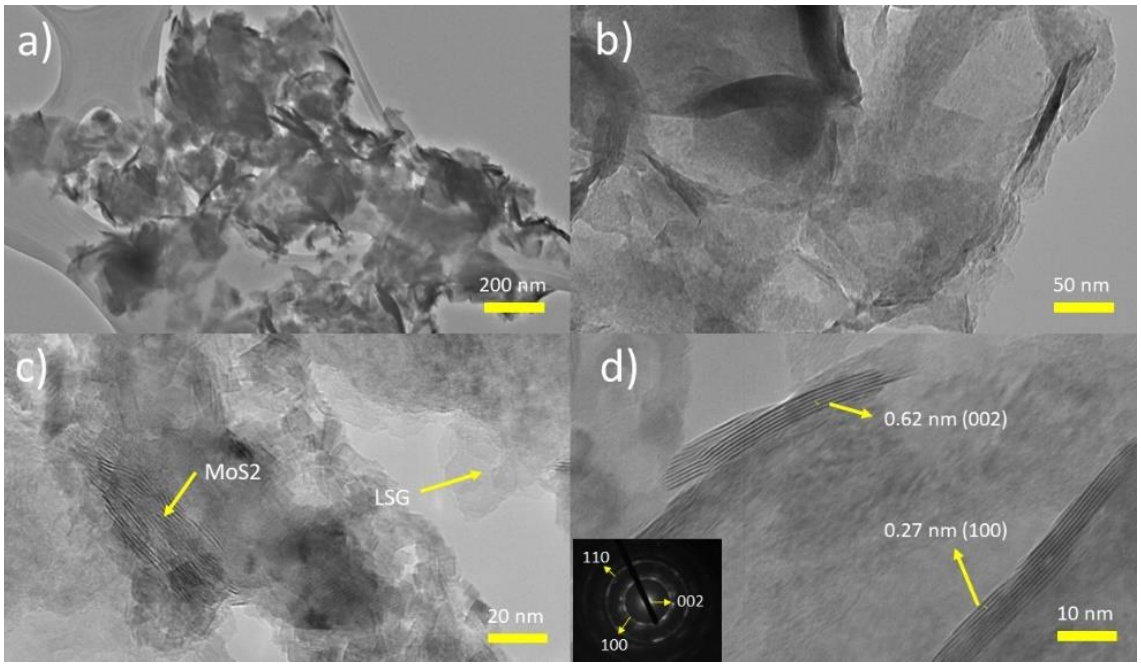

Fig. 3: (a) Typical TEM image of MoS_2 decorated on the surface of LSG. b) High magnification TEM image. (c & d) High-Resolution TEM image showing the lattice fringes of LSG and MoS_2 with the addition of the SAED pattern.

in width were found, However, these grains are densely packed and overlapped with each other, preventing an accurate lattice symmetry. Single stripe-like grain reveals 62 individual atomic planes ordered in the S–Mo–S sequence to form each layer. The carbon surface with a lighter color contrast under TEM confirms the hexagonal arrangement of S-Mo-S atoms. Part of the MoS_2 layer is vertically aligned, resulting in exposed molybdenum or sulfur atoms, which is beneficial for the higher catalytic activity of the MoS_2 sheets [34]. The high-resolution TEM image in Fig. 3d shows that the LSG layers covered with MoS_2 nanostructures with lattice spacing of 0.62 and 0.27nm, of the (002) and (100) planes of MoS_2, in agreement with the XRD results. The SAED pattern in Fig. 3d has several diffraction rings that corresponded well to MoS_2 planes. These results show that MoS_2 nanostructures on the LSG layer have good crystallinity [33].

X-ray diffraction (XRD)

An X-ray diffraction analysis was carried out to examine the crystallinity and plane orientation of LSG/MoS_2-1.0, as shown in Fig. 4. Fig. 4(a) displays the peak of Laser Scribe Graphene at 25°, indicating the successful formation of LSG. For pure MoS_2 in Fig. 4(b), the diffraction peaks are well matched with Joint Committee on Powder Diffraction Standards (JCPDS) Card No. 37-1492. The peaks appear at 14.2°, 33.5°, 43.1°, and 59.3°, corresponding to (002), (100), (103), and (110) planes originating from stacking layers and confirming the layered structure of MoS_2 [23]. For LSG/MoS_2-1.0 nanocomposite in Fig. 4(c), all of the characteristic peaks of pure MoS_2 are present, which suggests the same atomic arrangement along the basal planes of MoS_2 in LSG/MoS_2-1.0. There is no obvious peak for the LSG component due to the composite hybrid dominant by MoS_2. Only the broad peak observed at 2°- 24.30° indicates the presence of LSG layers [16]. All these indicative diffraction features could be used to confirm the presence of LSG wrapped with the formation of few-layer MoS_2 structures in the LSG/MoS_2-1.0 hybrid.

Fourier Transform Infrared Spectroscopy (FT-IR)

FT-IR analysis was conducted to determine the functional groups of the prepared materials. Fig. 5 depicts the FT-IR spectra of lignin-based graphene (Fig. 5a), MoS_2 (Fig. 5b) and LSG/MoS_2-1.0 (Fig. 5c). The absorption peaks of LSG/MoS_2-1.0 are distinct at 3450 cm^{-1}, 1700 cm^{-1}, 1430 cm^{-1}, 1125 cm^{-1},752 cm^{-1} and 650 cm^{-1}, which

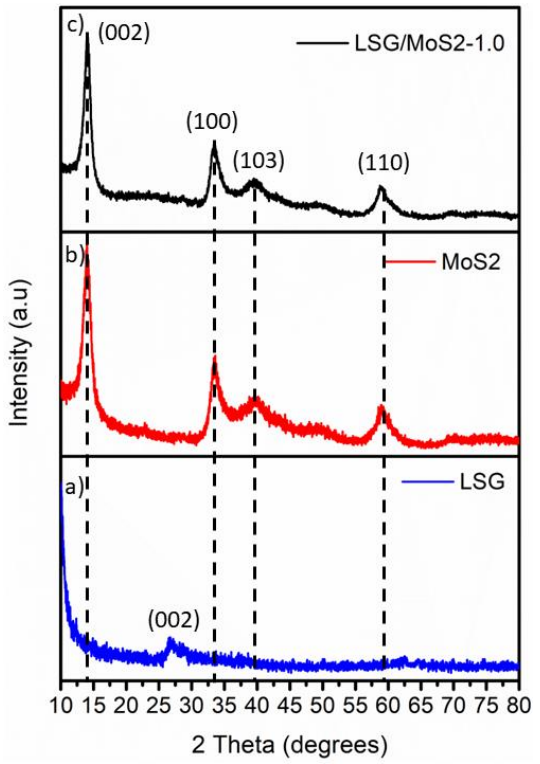

Fig. 4: (a) X-ray diffraction spectra of (a) LSG; (b) MoS_2 nanoflower and (c) LSG/MoS_2-1.0. Showing the crystalline peaks of fabricated nanostructures.

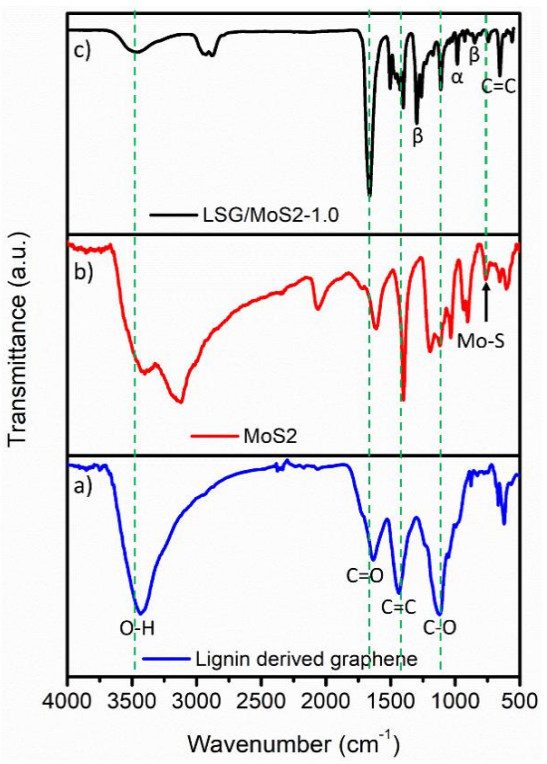

Fig. 5: FT-IR spectra of (a) lignin-based graphene; (b) MoS_2 and (c) LSG/MoS_2-1.0.

assigned to O-H, C=O, C=C, C-O, Mo-S and C=C groups, respectively [23,35,36]. The 1700 cm^{-1} peak also contributes to the C=C stretching vibration of carbon black [37]. The broad O-H bond (hydroxyl) at 3450 cm^{-1} is almost similar for all fabricated materials and is caused by the adsorption of water molecules. The presence of PVDF confirms the existence of α and β phases. The β phase peaks are 1400 cm^{-1} and 840 $cm^{-1,}$ while the IR vibration modes of α phases are 975 cm^{-1} [38]. The FT-IR analysis of LSG/MoS_2-1.0 has validated the successful pairing of LSG and MoS_2 in the fabricated material.

X-ray Photoelectron Spectroscopy (XPS)

XPS was conducted to study the elemental composition and chemical present on the outmost layer of grown MoS_2 nanoflower on the LSG surface. As expected, the survey scan of the LSG/MoS_2-1.0 has photoelectron peaks of carbon (C), oxygen (O), molybdenum (Mo), sulfur (S), and fluorine (F), as shown in Fig. 6a. The carbon, C1s spectrum (Fig. 6b) of LSG/MoS_2-1.0 have peaks at 284.3 eV (C=C and sp^2 carbon), 285.5 eV (sp^3 carbon), 286.5 eV (C-O), 287.8 eV (C=O), 289.2 eV (O-C=O), 291.2 eV (CF_2) and 292.9 eV (CF_3) [39–41]. These peaks correspond to the presence of graphene and the interactions of carbon atoms with oxygen, forming carbonyl and epoxide functional groups found at the graphene edges. The epoxy functional groups determine the defects and disorder of graphene structure in the basal plane. The formation of CF_2 and CF_3 proves that PVDF is merged with carbon bonds forming LSG [42]. The oxygen, O1s spectra displayed in Fig. 6c showed peaks of carbonyl (C=O) at 534.2 eV, carboxylic group (COOH) at 531.4 eV, hydroxyl or ethers (C-O) at 532.7 eV and chemisorbed oxygen in C-OH [22]. The carboxyl and carbonyl groups in LSG/MoS_2-1.0 boosts the electrochemical performance of the sensor by enhancing the wettability of the electrode and electron diffusion rate. The enlarged spectra of Mo 3d are in Fig. 6d and can be deconvoluted to binding energy peaks at 228.6, 231.9, and 235.6 eV, which are assigned to Mo^{4+} $3d_{5/2}$, Mo^{4+} $3d_{3/2,}$ and Mo^{6+} $3d_{3/2}$, respectively [43,44]. The formation of MoS_2 is identified from the presence of Mo^{4+}. However, the Mo^{6+} is from the surface oxidized

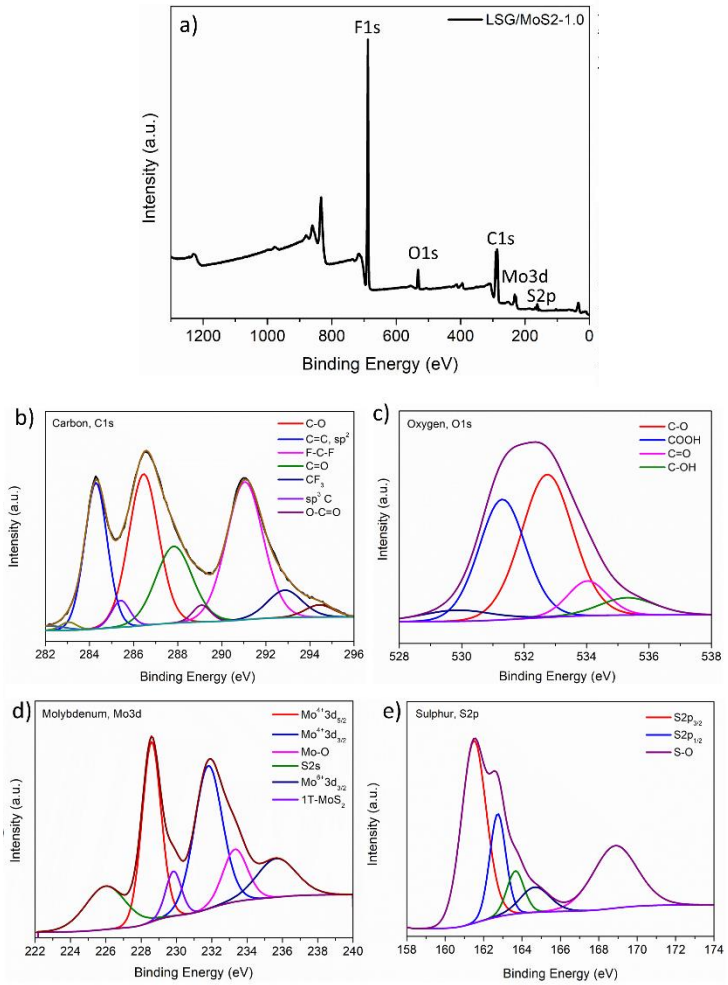

Fig. 6: XPS spectra of LSG/MoS_2-1.0 (a) Survey scan; (b) Carbon, C1s; (c) Oxygen, O1s; (d) Molybdenum, Mo3d; and (e) Sulphur, S2p.

and the unconverted molybdenum residues in the precursor forming the Mo-O group at peaks 233.4 eV. The Mo^{4+} peaks confirm the formation of 2H-MoS_2 (semiconductor), whereas a peak at 229.8 eV refers to 1T-MoS2 (metallic). S 2s orbital was also observed at 226 eV [45]. The XPS spectra of three characteristic peaks of S 2p at 161.5 (S $2p_{3/2}$), 162.7 (S $2p_{1/2}$), and 169 (S-O) eV in Fig. 6e reveal the presence of sulfur. The S-O bond appeared during the formation of MoS_2 nanoflower. The XPS analysis confirms the existence and interactions in the LSG/MoS_2-1.0.

Electrochemical Impedance Spectroscopy (EIS)

EIS was carried out to investigate the electrochemical performance of LSG/MoS_2 hybrids on the surface of screen-printed electrode (SPE) chips at room temperature. Fig. 7 shows the Nyquist plot indicating the impedance of the material tested under an initial frequency of 1 MHz and a final frequency of 150Hz. The diameter of the semicircle arc corresponds to the resistance transfer charge (Rct) due to the combination of the double-layer capacitance and Faradic reactions [46]. The lignin-based graphene with an absence of modified materials like carbon black and PVDF has an Rct value of 100K, as shown in Fig. 7a. The unavoidable residue of lignin in scribed graphene and the amorphous nature of lignin causes the resistivity to be high [47]. In Fig. 7b, the values of Rct obtained for LSG/MoS_2-1.0, LSG/MoS_2-0.5, LSG/MoS_2-0.1, MoS_2 and LSG electrodes are 13KΩ, 18KΩ, 27KΩ, 44KΩ, and 77KΩ, respectively. The modified LSG with the presence of carbon black, PVDF, and NMP reduces the resistivity and improves the electron transfer efficiency. As the addition of LSG increases in hybrids, the capacitive

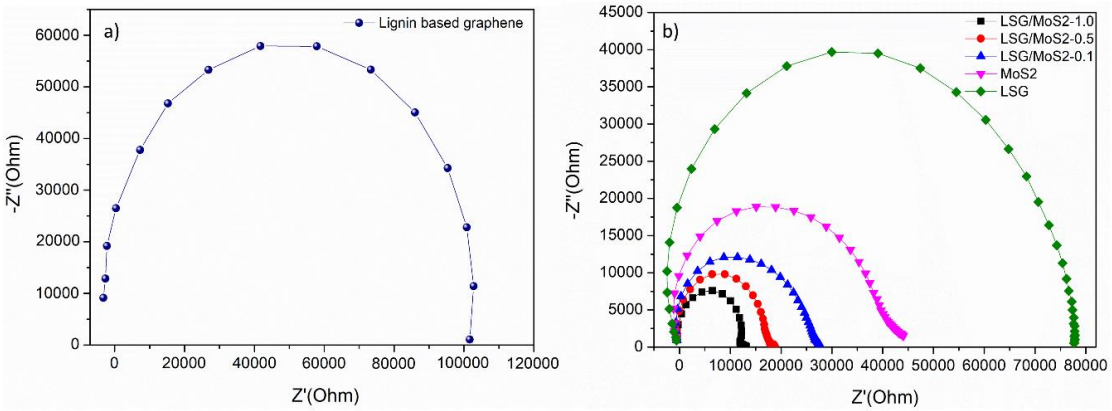

Fig. 7: Nyquist plot of (a) lignin-based graphene and (b) composite nanomaterials.

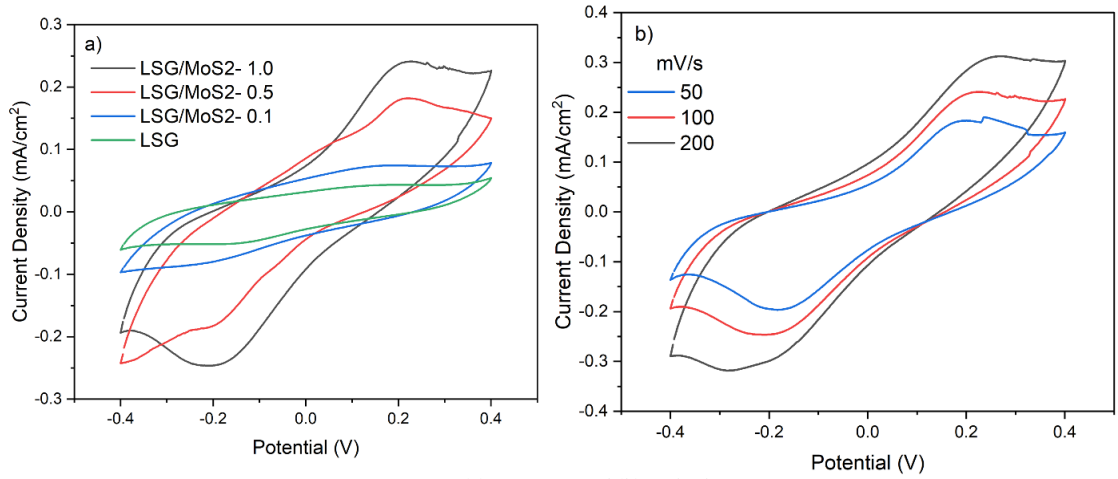

Fig. 8: CV curves (a) 100 mV/s and (b) multiple scan rates.

behavior improves, with LSG/MoS_2-1.0 having the best capacitive and electrical conductivity. The reduction in the diameter of the semicircle arc in the hybrid material indicates a significant decrease in transfer resistance, enhanced redox reaction of charge and discharge, and higher flexibility of the polymer chain for intercalation [30,48]. The increase in graphene increases the surface area, which enhances the number of charges carried. Furthermore, the anchored MoS_2 nanoflower prevents the zero band gap of Laser Scribed Graphene layers, and the loosely-formed open pores structures promote quick electron transmission between the active material and the charge collector [49]. The EIS results revealed LSG/MoS_2-1.0 hybrid attribute to the improved storage and transport of charges within the electrode compared to other concentrations for potential supercapacitor application [50,51].

Cyclic Voltammetry (CV)

The capacitive properties of fabricated graphene were further investigated through Cyclic Voltammetry analysis at a voltage range of -0.4V to 0.4V. The graph presented in Fig. 8 (a) shows all CV plots obtained at a scan rate of 100 mV/s exhibit a redox peak, attributed to the presence of both MoS_2 nanoflowers and lignin-derived aromatics in the composites [52,53]. Notably, the composite with a greater amount of LSG shows a more pronounced redox peak, indicating a more significant contribution from the lignin aromatics to the redox behavior of the composite. According to the CV reading from SPE chips, LSG/MoS_2-1.0 has the maximum areal capacitance (1.72 mF/cm^2), followed by other composite materials with lower and zero concentrations of LSG with MoS_2 nanoflowers (1.25, 0.73, and 0.48 mF/cm^2). The facilitation of charge transfer from the edges to

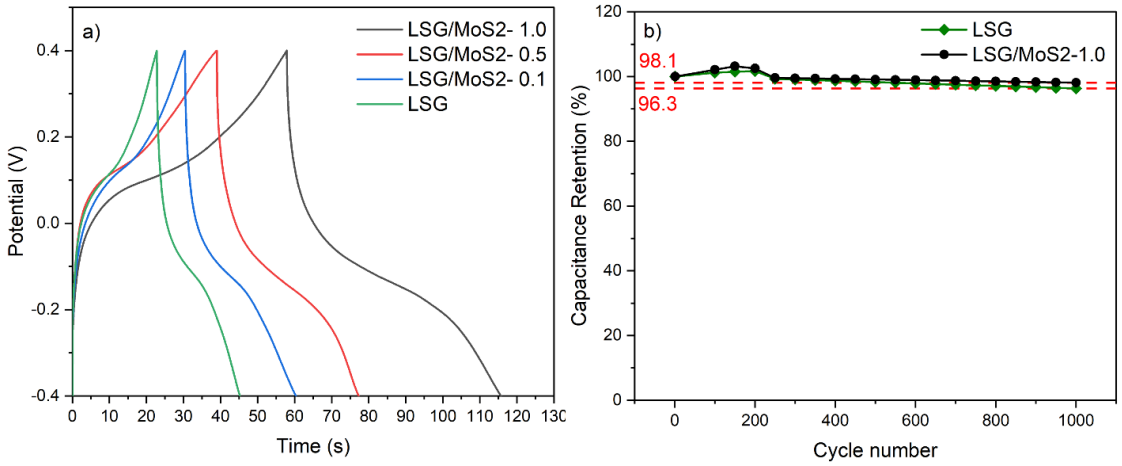

Fig. 9: (a) GCD curves of LSG and composite nanomaterials at 0.05 mA/cm^2; (b) Cyclic performance of LSG and composite nanomaterials.

the inner core of the material has been improved by the higher surface area and strong electrical conductivity capabilities of MoS_2 nanoflowers [46]. Fig. 8 (b) compares the LSG/MoS_2-1.0 electrode at various scan rates, demonstrating faster and slower charging and discharging processes because of the shift in exposure time.

Galvanostatic Charge and Discharge (GCD)

Fig. 9 (a) shows the charge and discharge curves of fabricated graphene and composite material at a current density of 0.05 mA/cm^2. The irregular triangle-shaped charge/discharge curves of both ordinary and composite materials were strongly impacted by the pseudocapacitive characteristics of the aromatic compounds present on lignin and from the fabricated MoS_2 nanoflower. The GCD-specific capacitances of LSG and composite electrodes are 2.42, 3.18, 4.17, and 6.7 mF/cm^2 at increasing LSG mass. The composite containing the largest quantity of LSG (LSG/MoS_2-1.0) has the best capacitive properties. This is attributed to the combination of an electric double-layer capacitance (ELDC) and a pseudocapacitance material, forming a highly conductive composite in the presence of MoS_2 nanoflowers. The cyclic performance of ordinary LSG and LSG/MoS_2-1.0 were examined at 0.1 mA/cm^2 for 1000 charge/discharge cycles (Fig. 9 (b)). LSG/MoS_2-1.0 recorded the highest cyclic stability of 98.1%, indicating that the addition of MoS_2 nanoflowers has improved the quality of the LSG.

CONCLUSION

Oil palm lignin was successfully converted into Laser Scribed Graphene (LSG) at a lignin concentration of 20%, laser power of 50%, and laser speed of 50%. The converted 3D LSG has high graphene quality. Besides that, the hybrid LSG/MoS_2 nanostructure and 3D MoS_2 nanoflower were successfully fabricated through a finely tuned hydrothermal method. Morphology analyses have been conducted for all the synthesized nanomaterials. The electrochemical characterization of hybrids revealed that LSG/MoS_2-1.0 has the ideal capacitance behavior and high electrical conductivity with low resistivity. The incorporation of the optimized ratio of EDLC (LSG) to Faradaic (MoS_2) material to form a promising hybrid material resulted in LSG/MoS2-1.0 having the highest areal capacitance and capacitance retention of 6.7mF/cm^2 and 98.1%. The development and enhancement of graphene from green materials such as lignin would create a new path for green electronics, specifically high-performing supercapacitors.

ACKNOWLEDGMENTS

This research is supported by the Ministry of Higher Education Malaysia Fundamental Research Grant Scheme (FRGS) (FRGS/1/2020/TKO/UTP/03/7). The Nanotechnology Research Laboratory and Dye Solar Cell Laboratory, Universiti Teknologi PETRONAS (UTP), provided the testing facilities.

CONFLICT OF INTEREST

The authors hereby declare that there is no conflict of interest.

REFERENCES

[1] H.H. Hsu, W. Zhong, Nanocellulose-based conductive membranes for free-standing supercapacitors: A review, Membranes (Basel). 9 (2019). https://doi.org/10.3390/membranes9060074.

[2] P.K. Kalambate, R.A. Dar, S.P. Karna, A.K. Srivastava, High performance supercapacitor based aon graphene-silver nanoparticles-polypyrrole nanocomposite coated on glassy carbon electrode, J. Power Sources. 276 (2015) 262-270. https://doi.org/10.1016/j.jpowsour.2014.11.130.

[3] O.K. Oyeniran, H. Pretoria, Synthesis and characterization of carbon-based nanostructured material electrodes for designing novel hybrid supercapacitors, 2018.

[4] M.J.Y. Tai, M. Vasudevan, V. Perumal, W.W. Liu, N.M. Mohamed, Synthesis of Laser Scribed Graphene Electrode with Optimized Power for Biosensing, in: Proc. 2019 IEEE Reg. Symp. Micro Nanoelectron. RSM 2019, 2019. https://doi.org/10.1109/RSM46715.2019.8943572.

[5] S.-K. Hyeong, K.-H. Choi, S.-W. Park, S. Bae, M. Park, S. Ryu, J.-H. Lee, S.-K. Lee, Review of the Direct Laser Synthesis of Functionalized Graphene and its Application in Sensor Technology, Appl. Sci. Converg. Technol. 28 (2019) 148-154. https://doi.org/10.5757/asct.2019.28.5.148.

[6] Z. Wan, X. Chen, M. Gu, Laser scribed graphene for supercapacitors, Opto-Electronic Adv. 4 (2021). https://doi.org/10.29026/oea.2021.200079.

[7] N.N. Loganathan, K.R. Munusamy, V. Perumal, B.R. Pandian, Laser scribed graphene from oil palm lignin for supercapacitor applications, J. Water Environ. Nanotechnol. 6 (2021) 356-366. https://doi.org/10.22090/jwent.2021.04.006.

[8] R. Dungani, P. Aditiawati, S. Aprilia, K. Yuniarti, T. Karliati, I. Suwandhi, I. Sumardi, Biomaterial from Oil Palm Waste: Properties, Characterization and Applications, in: Palm Oil, InTech, 2018. https://doi.org/10.5772/intechopen.76412.

[9] L.S. Anthony, M. Vasudevan, V. Perumal, M. Ovinis, P.B. Raja, T.N.J.I. Edison, Bioresource-derived polymer composites for energy storage applications: Brief review, J. Environ. Chem. Eng. 9 (2021). https://doi.org/10.1016/j.jece.2021.105832.

[10] M. Vasudevan, M.J.Y. Tai, V. Perumal, S.C.B. Gopinath, S.S. Murthe, M. Ovinis, N.M. Mohamed, N. Joshi, Cellulose acetate-MoS<inf>2</inf> nanopetal hybrid: A highly sensitive and selective electrochemical aptasensor of Troponin I for the early diagnosis of Acute Myocardial Infarction, J. Taiwan Inst. Chem. Eng. 118 (2021). https://doi.org/10.1016/j.jtice.2021.01.016.

[11] D. Wang, Z. Pan, Z. Wu, Z. Wang, Z. Liu, Hydrothermal synthesis of MoS2 nanoflowers as highly efficient hydrogen evolution reaction catalysts, J. Power Sources. 264 (2014) 229-234. https://doi.org/10.1016/j.jpowsour.2014.04.066.

[12] M. Govindasamy, S.M. Chen, V. Mani, M. Akilarasan, S. Kogularasu, B. Subramani, Nanocomposites composed of layered molybdenum disulfide and graphene for highly sensitive amperometric determination of methyl parathion, Microchim. Acta. 184 (2017) 725-733. https://doi.org/10.1007/s00604-016-2062-6.

[13] I.T. Bello, K.O. Otun, G. Nyongombe, O. Adedokun, G.L. Kabongo, M.S. Dhlamini, Synthesis , Characterization , and Supercapacitor Performance of a Mixed-Phase Mn-Doped MoS 2 Nanoflower, Nanomaterials. 12 (2022) 1-12. https://doi.org/10.3390/nano12030490

[14] M.A. Bissett, I.A. Kinloch, R.A.W. Dryfe, Characterization of MoS2-Graphene Composites for High-Performance Coin Cell Supercapacitors, ACS Appl. Mater. Interfaces. 7 (2015) 17388-17398. https://doi.org/10.1021/acsami.5b04672.

[15] S.K. Asl, M.N. Habashi, A. Kianvash, A. Alipour, S. Mohini, Fabrication of Graphene / MoS 2 Nanocomposite for Flexible Energy Storage, J. Nanostructures. 9 (2019) 21-28. https://doi.org/10.22052/JNS.2019.01.004.

[16] M.M. Baig, E. Pervaiz, M. Yang, I.H. Gul, High-Performance Supercapacitor Electrode Obtained by Directly Bonding 2D Materials: Hierarchal MoS2 on Reduced Graphene Oxide, Front. Mater. 7 (2020). https://doi.org/10.3389/fmats.2020.580424.

[17] F. Ghasemi, M. Jalali, A. Abdollahi, S. Mohammadi, Z. Sanaee, S. Mohajerzadeh, A high performance supercapacitor based on decoration of MoS2/reduced graphene oxide with NiO nanoparticles, RSC Adv. 7 (2017) 52772-52781. https://doi.org/10.1039/c7ra09060a.

[18] M.J.Y. Tai, V. Perumal, S.C.B. Gopinath, P.B. Raja, M.N.M. Ibrahim, I.N. Jantan, N.S.H. Suhaimi, W.W. Liu, Laser-scribed graphene nanofiber decorated with oil palm lignin capped silver nanoparticles: a green biosensor, Sci. Rep. 11 (2021) 1-9. https://doi.org/10.1038/s41598-021-85039-2.

[19] S. Rajeevan, S. John, S.C. George, The effect of poly(vinylidene fluoride) binder on the electrochemical performance of graphitic electrodes, J. Energy Storage. 39 (2021) 102654. https://doi.org/10.1016/j.est.2021.102654.

[20] S. Sopčić, M.K. Roković, Z. Mandić, Preparation and characterization of ruo2/polyaniline/polymer binder composite electrodes for supercapacitor applications, J. Electrochem. Sci. Eng. 2 (2012) 41-52. https://doi.org/10.5599/jese.2012.0010.

[21] S. Zhang, C. Lum, N. Pan, Enhanced performance of carbon/carbon supercapacitors upon graphene addition, Nanotechnol. Environ. Eng. 2 (2017) 1-8. https://doi.org/10.1007/s41204-017-0020-0.

[22] I.I.G. Inal, Scalable activated carbon/graphene based supercapacitors with improved capacitance retention at high current densities, Turkish J. Chem. 45 (2021) 927-941. https://doi.org/10.3906/kim-2012-39.

[23] M. Vasudevan, M.J.Y. Tai, V. Perumal, S.C.B. Gopinath, S.S. Murthe, M. Ovinis, N.M. Mohamed, N. Joshi, Highly sensitive and selective acute myocardial infarction detection using aptamer-tethered MoS<inf>2</inf> nanoflower and screen-printed electrodes, Biotechnol. Appl. Biochem. 68 (2021). https://doi.org/10.1002/bab.2060.

[24] K. Gobalu, M. Vasudevan, S.C.B. Gopinath, V. Perumal, M. Ovinis, Molybdenum disulphide/cellulose acetate nanofiber composite on screen printed electrodes for detecting cardiac troponin by electrical impedance spectroscopy, Cellulose. 28 (2021). https://doi.org/10.1007/s10570-021-03911-w.

[25] D. Chen, W. Chen, L. Ma, G. Ji, K. Chang, J.Y. Lee, Graphene-like layered metal dichalcogenide/graphene

composites: Synthesis and applications in energy storage and conversion, Mater. Today. 17 (2014) 184-193. https://doi.org/10.1016/j.mattod.2014.04.001.

[26] J. Chen, B. Yao, C. Li, G. Shi, An improved Hummers method for eco-friendly synthesis of graphene oxide, Carbon N. Y. 64 (2013) 225-229. https://doi.org/10.1016/j.carbon.2013.07.055.

[27] E. Ghoniem, S. Mori, A. Abdel-Moniem, Low-cost flexible supercapacitors based on laser reduced graphene oxide supported on polyethylene terephthalate substrate, J. Power Sources. 324 (2016) 272-281. https://doi.org/10.1016/j.jpowsour.2016.05.069.

[28] M.N. Habashi, S.K. Asl, Flexible Micro Supercapacitor Based on Laser Scribed Graphene (LSG) Fabrication of doped TiO2 nanotube array films with enhanced photo-catalytic activity View project electroceramics: piezoelectrics, conductors, semiconductors and magnetic materials View project, 2018. www.scholarena.com.

[29] G.A.M. Ali, M.R. Thalji, W.C. Soh, H. Algarni, K.F. Chong, One-step electrochemical synthesis of MoS2/graphene composite for supercapacitor application, J. Solid State Electrochem. 24 (2020) 25-34. https://doi.org/10.1007/s10008-019-04449-5.

[30] W. Zhang, Y. Lei, Q. Jiang, F. Ming, P.M.F.J. Costa, H.N. Alshareef, 3D Laser Scribed Graphene Derived from Carbon Nanospheres: An Ultrahigh-Power Electrode for Supercapacitors, Small Methods. 3 (2019). https://doi.org/10.1002/smtd.201900005.

[31] F. Mahmood, F. Mahmood, H. Zhang, J. Lin, C. Wan, Laser-Induced Graphene Derived from Kraft Lignin for Flexible Supercapacitors, ACS Omega. 5 (2020) 14611-14618. https://doi.org/10.1021/acsomega.0c01293.

[32] H. Yoon, J. Nah, H. Kim, S. Ko, S.C. Barman, X. Xuan, J. Kim, J.Y. Park, Sensors and Actuators B : Chemical A chemically modified laser-induced porous graphene based flexible and ultrasensitive electrochemical biosensor for sweat glucose detection, 311 (2020).
https://doi.org/10.1016/j.snb.2020.127866

[33] Y. Zhong, T. Shi, Y. Huang, S. Cheng, C. Chen, G. Liao, Z. Tang, Three-dimensional MoS2/Graphene Aerogel as Binder-free Electrode for Li-ion Battery, Nanoscale Res. Lett. 14 (2019). https://doi.org/10.1186/s11671-019-2916-z.

[34] X. Zhang, M. Zhang, Y. Tian, J. You, C. Yang, J. Su, Y. Li, Y. Gao, H. Gu, In situ synthesis of MoS2/graphene nanosheets as free-standing and flexible electrode paper for high-efficiency hydrogen evolution reaction, RSC Adv. 8 (2018) 10698-10705. https://doi.org/10.1039/c8ra01226a.

[35] C.R.- Graphene, M.A. Aldosari, K. Bin, B. Alsaud, A. Othman, M. Al-hindawi, N.H. Faisal, R. Ahmed, F.M. Michael, M.R. Krishnan, Microwave Irradiation Synthesis and Nanoparticle Nanocomposites and Their Anti-Microbial Activity, Polymers (Basel). 12, 1155 (2020) 1-16.
https://doi.org/10.3390/polym12051155

[36] R. Vinoth, I.M. Patil, A. Pandikumar, B.A. Kakade, N.M. Huang, D.D. Dionysios, B. Neppolian, Synergistically Enhanced Electrocatalytic Performance of an N - Doped Graphene Quantum Dot-Decorated 3D MoS 2 – Graphene Nanohybrid for Oxygen Reduction Reaction, ACS Omega. 1 (2016) 971-980. https://doi.org/10.1021/acsomega.6b00275.

[37] C.D. Zappielo, D.M. Nanicuacua, W.N.L. Dos Santos, D.L.F. Da Silva, L.H. Dall'antônia, F.M. De Oliveira, D.N. Clausen, C.R.T. Tarley, Solid Phase Extraction to On-Line Preconcentrate Trace Cadmium Using Chemically Modified Nano-Carbon Black with 3-Mercaptopropyltrimethoxysilane, J. Braz. Chem. Soc. 27 (2016) 1715-1726. https://doi.org/10.5935/0103-5053.20160052.

[38] I.Y. Abdullah, M. Yahaya, M.H.H. Jumali, H.M. Shanshool, Effect of annealing process on the phase formation in Poly(vinylidene fluoride) thin films, AIP Conf. Proc. 1614 (2014) 147-151. https://doi.org/10.1063/1.4895187.

[39] A.A. Dolgov, T.F. Scientific, D. Lopaev, C.J. Lee, H. Fontys, E. Zoethout, Characterization of carbon contamination under ion and hot atom bombardment in a tin-plasma extreme ultraviolet light source, Appl. Surf. Sci. 353 (2015) 708-713. https://doi.org/10.1016/j.apsusc.2015.06.079.

[40] N. Akashi, S. Kuroda, Protein immobilization onto poly (vinylidene fluoride) microporous membranes activated by the atmospheric pressure low temperature plasma Protein immobilization onto poly (vinylidene fl uoride) microporous membranes activated by the atmospheric pressu, Polymer (Guildf). 55 (2015) 2780-2791. https://doi.org/10.1016/j.polymer.2014.04.029.

[41] P. Viswanath, M. Yoshimura, Light - induced reversible phase transition in polyvinylidene fluoride - based nanocomposites, SN Appl. Sci. 1 (2019) 1-9. https://doi.org/10.1007/s42452-019-1564-3.

[42] Z. Cui, Polymers EVOH in situ fibrillation and its effect of strengthening , toughening and hydrophilic modification on PVDF hollow fiber microfiltration membrane via TIPS process, J. Mater. Sci. 54 (2019) 5971-5987. https://doi.org/10.1007/s10853-018-03281-y.

[43] R. Amin, A. Hossain, Y. Zakaria, Interfacial Kinetics and Ionic Diffusivity of the Electrodeposited MoS2 Film Interfacial Kinetics and Ionic Di ff usivity of the Electrodeposited MoS 2 Film, Appl. Mater. Interfaces. 10 (2018) 16. https://doi.org/10.1021/acsami.8b01104.

[44] A. Duan, Z. Zhao, G. Jiang, J. Liu, Catalytic performance and sulfidation behaviors of CoMo / Beta-MCM-48 catalysts prepared with citric acid for FCC gasoline hydroupgrading, J. Porous Mater. 22 (2015) 1. https://doi.org/10.1007/s10934-014-9879-3.

[45] B. Li, L. Jiang, X. Li, P. Ran, P. Zuo, A. Wang, L. Qu, Y. Zhao, Preparation of Monolayer MoS 2 Quantum Dots using Temporally Shaped Femtosecond Laser Ablation of Bulk MoS 2 Targets in Water, Sci. Rep. 7 (2017) 1-12. https://doi.org/10.1038/s41598-017-10632-3.

[46] L.Q. Fan, G.J. Liu, C.Y. Zhang, J.H. Wu, Y.L. Wei, Facile one-step hydrothermal preparation of molybdenum disulfide/carbon composite for use in supercapacitor, Int. J. Hydrogen Energy. 40 (2015) 10150-10157. https://doi.org/10.1016/j.ijhydene.2015.06.061.

[47] S.H. Sekeri, M.N.M. Ibrahim, K. Umar, A.A. Yaqoob, M.N. Azmi, M.H. Hussin, M.B.H. Othman, M.F.I.A. Malik, Preparation and characterization of nanosized lignin from oil palm (Elaeis guineensis) biomass as a novel emulsifying agent, Int. J. Biol. Macromol. 164 (2020) 3114-3124. https://doi.org/10.1016/j.ijbiomac.2020.08.181.

[48] D. Gupta, V. Chauhan, R. Kumar, A comprehensive review

on synthesis and applications of molybdenum disulfide (MoS2) material: Past and recent developments, Inorg. Chem. Commun. 121 (2020). https://doi.org/10.1016/j.inoche.2020.108200.

[49] K.J. Huang, L. Wang, Y.J. Liu, Y.M. Liu, H.B. Wang, T. Gan, L.L. Wang, Layered MoS2-graphene composites for supercapacitor applications with enhanced capacitive performance, Int. J. Hydrogen Energy. 38 (2013) 14027-14034. https://doi.org/10.1016/j.ijhydene.2013.08.112.

[50] J. Bao, X.F. Zeng, X.J. Huang, R.K. Chen, J.X. Wang, L.L. Zhang, J.F. Chen, Three-dimensional MoS2/rGO nanocomposites with homogeneous network structure for supercapacitor electrodes, J. Mater. Sci. 54 (2019) 14845-14858. https://doi.org/10.1007/s10853-019-03957-z.

[51] X. Yuan, X. Li, X. Zhang, Y. Li, L. Liu, MoS2 vertically grown on graphene with efficient electrocatalytic activity in Pt-free dye-sensitized solar cells, J. Alloys Compd. 731 (2018) 685-692. https://doi.org/10.1016/j.jallcom.2017.08.208.

[52] B. Zhou, W. Liu, Y. Gong, L. Dong, Y. Deng, High-performance pseudocapacitors from kraft lignin modified active carbon, Electrochim. Acta. 320 (2019) 134640. https://doi.org/10.1016/j.electacta.2019.134640.

[53] M. Fu, Z. Zhu, W. Chen, H. Yu, Q. Liu, Microwave-assisted synthesis of MoS2/graphene composites for supercapacitors, J. Mater. Sci. 55 (2020) 16385-16393. https://doi.org/10.1007/s10853-020-05201-5.